Transport effects in non-Hermitian nonreciprocal systems: General approach

Hamed Ghaemi-Dizicheh **

Department of Physics and Astronomy, University of Texas Rio Grande Valley, Edinburg, Texas 78539, USA

(Received 10 December 2022; revised 6 February 2023; accepted 20 March 2023; published 28 March 2023)

In this paper, we present a unifying analytical framework for identifying conditions for transport effects such as reflectionless and transparent transport, lasing, and coherent perfect absorption in non-Hermitian nonreciprocal systems using a generalized transfer matrix method. This provides a universal approach to studying the transport of tight-binding platforms, including higher-dimensional models and those with an internal degree of freedom going beyond the previously studied case of one-dimensional chains with nearest-neighbor couplings. For a specific class of tight-binding models, the relevant transport conditions and their signatures of non-Hermitian, nonreciprocal, and topological behavior are analytically tractable from a general perspective. We investigate this class and illustrate our formalism in a paradigmatic ladder model where the system's parameters can be tuned to adjust the transport effect and topological phases.

DOI: 10.1103/PhysRevB.107.125155

I. INTRODUCTION

In recent years, the study of topological models has been extended to non-Hermitian Hamiltonians, which appear as effective Hamiltonians of open systems or wave systems with gain and loss [1-3]. The appearance of nonreciprocity introduces another non-Hermitian extension, which gives rise to novel phenomena such as the non-Hermitian skin effect (NHSE) [4–10] and the recently identified edge burst effect [11]. In the former effect, the bulk states become localized at the edge of a finite system with open boundary conditions, a behavior that is drastically different from its periodic counterpart. In the latter effect, a substantial portion of loss occurs at the system boundary.

In addition, incorporating non-Hermitian topological models into photonics systems has introduced novel platforms known as topological photonics [12-14], which can induce a rich diversity of transport phenomena such as lasing [15–19], coherent perfect absorption [20-22], reflectionless scattering [23], invisibility [24], and transparency [25].

Hence, developing a formulation for the distinct transport effects in non-Hermitian nonreciprocal systems paves the way toward investigating interesting phenomena in such platforms. Following this motivation in our previous paper, we studied (i) conditions for variant transport effects, (ii) their compatibility with each other, and (iii) their adjustment by tuning suitable parameters facilitated by symmetry or topology [26]. We then found distinct transport signatures of non-Hermitian, nonreciprocal, and topological systems. For instance, (i) the direction of reflectionless transport depends on the topological phases, (ii) invisibility coincides with the non-Hermitian skin-effect phase transition of topological edge states, and (iii) a unidirectional transparent coherent perfect absorption emerges.

Our previous study considered a generic one-dimensional chain with nearest-neighbor couplings. However, this study can be further generalized to more involved models. Here, we address this generalization to analytically formulate the spectral conditions for a range of distinct phenomena and identify their interdependence.

Our method is based on exploiting the transfer matrix [27] to characterize the transport boundary conditions. Along with the scattering matrix [28], the transfer matrix is a prominent mathematical instrument to study transport in finite-range scattering potentials. Recently, a developed version of the transfer matrix method has established itself as an analytic approach in non-Hermitian tight-binding models to study topological [29,30] and localization phenomena [31].

In Ref. [26], we employed the transfer matrix to define transport boundary conditions and their connection. Following the same formulation, we can extend the derivation of the transfer matrix describing transportation in a general nonreciprocal lattice. This approach can provide a universal characterization of various transport phenomena.

We then consider a class of nonreciprocal tight-binding systems whose transport signatures are described by a 2×2 transfer matrix. We will show that our conclusions in [26] for the transport effects and their compatibility can be retrieved in a general context for all those models settled in this specific category.

The rest of this paper is organized as follows: we describe our method for constructing the transfer matrix for a general tight-binding model in real and propagating space in Sec. II, where we present a global scheme of the leads in Fig. 1. We then determine the boundary conditions of distinct transport effects and their interplay in Sec. III with a general attitude. In Sec. IV, we investigate our general formalism for a class of systems whose transfer matrix reduces to a 2×2 matrix that is familiar in the photonics models. For these models, we can categorize the transport boundary conditions as implicit equations in terms of the parameters, possibly associated with

^{*}hghaemidizicheh@ku.edu.tr

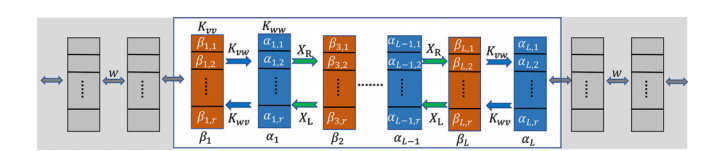


FIG. 1. A schematic diagram of the recursion relations (10) and (11) describing non-Hermitian nonreciprocal systems with q internal degrees of freedom and range of interaction \mathfrak{r} . This diagram represents a general tight-biding model connecting to the featureless leads (with coupling w < 0).

the topology and reciprocity of the system. To demonstrate our approach, we investigate the transport effect of the Ladder lattice. We then show that by generalizing the coupling parameters, the system can be tuned to be reflectionless in the nontrivial topological phase. This suggests that our research can be used to determine an appropriate set of system parameters for building a platform with specific transport effects in different topological phases.

II. MATHEMATICAL SETUP

A. Model of supercells

To extend the theory of transport from a rather simple one-dimensional chain to a more complicated structure, we consider a system that is described by a tight-binding model whose Hamiltonian is given by

$$\mathcal{H} = \sum_{n=1}^{N} \sum_{\alpha,\beta=1}^{q} \left[\sum_{l=1}^{\mathfrak{r}} (c_{n,\alpha}^{\dagger} [\mathbf{t}_{l}^{L}]_{\alpha\beta} c_{n+l,\beta} + c_{n+l,\alpha}^{\dagger} [\mathbf{t}_{l}^{R}]_{\alpha\beta} c_{n,\beta} + c_{n,\alpha}^{\dagger} [\mathbf{t}_{0}]_{\alpha\beta} c_{n,\beta} \right], \tag{1}$$

where $\mathbf{t}_{l}^{L(R)}$ denotes the hopping matrix to the left (right), and \mathbf{t}_{0} is the intra-unit-cell term. Also, in the Hamiltonian (1), the parameter \mathbf{r} is the range of hopping, and q determines the number of internal degrees of freedom, e.g., spin, orbital, or sublattice, per unit cell.

Following the main idea developed in [29,30], for the construction of the transfer matrix, we consider a bundle of \mathfrak{r} adjacent sites, which reduces the model with N cells to a supermodel with L supercells, each containing $\mathfrak{n}=q\mathfrak{r}$ degrees of freedom. Thus, the Hamiltonian of the superchain is given by

$$H = \sum_{n=1}^{2L} [\mathbf{c}_n^{\dagger} \mathbf{J}_L \mathbf{c}_{n+1} + \mathbf{c}_n^{\dagger} \mathbf{K} \mathbf{c}_n + \mathbf{c}_{n+1}^{\dagger} \mathbf{J}_R \mathbf{c}_n]. \tag{2}$$

Here, we introduce \mathbf{J}_L (\mathbf{J}_R) and \mathbf{K} , respectively, as the corresponding left (right) hopping and on-site matrices. The single-particle Schrödinger equation ($H\Psi=E\Psi$) is reduced to the following recursion relation:

$$E\Psi_n = \mathbf{K}\Psi_n + \mathbf{J}_R\Psi_{n-1} + \mathbf{J}_L\Psi_{n+1},\tag{3}$$

with $\Psi_n = (\psi_{2n-1}, \dots, \psi_{2n+\mathfrak{r}-1})^T \in \mathbb{C}^\mathfrak{n}$ defining the wave function for each supercell. In the case of reciprocal transport, one has $\mathbf{J}_R = \mathbf{J}_L^\dagger$, and the system is governed by a

Hermitian Hamiltonian with the real-valued spectrum provided that $\mathbf{K} = \mathbf{K}^{\dagger}$.

One can reduce the relation (3) by applying the reduced singular value decomposition (SVD) method [32] on both J_L and J_R . This reduction results in

$$\mathbf{J}_L = V X_L W^{\dagger}, \quad \mathbf{J}_R = W X_R V^{\dagger}, \tag{4}$$

where $X_{L/R} = \text{diag}\{\xi_{L/R}^1, \dots, \xi_{L/R}^r\}$ is a diagonal matrix of singular values $(\xi_{L/R}^{1,2,\dots,r})$ with $r := \text{rank}(\mathbf{J}_L)$, which is defined by the number of its independent rows. The columns of V and W are called the left- and right-singular vectors of \mathbf{J}_L [33]. We further require the size of the supercells to be big enough such that $\mathbf{J}_{L/R}$ becomes nilpotent of degree 2, i.e., $\mathbf{J}_{L/R}^2 = 0$. It then follows that $r \le q \mathbf{r}$ [29,30]. This condition leads to the following relations for left- and right-singular vectors:

$$V^{\dagger}V = W^{\dagger}W = \mathbb{1}_r, \quad V^{\dagger}W = 0, \tag{5}$$

where $\mathbb{1}_r$ is an $r \times r$ identity matrix. According to the above relation, span $\{V\}$ and span $\{W\}$ provide an orthonormal basis of \mathbb{C}^n such that Ψ_n can be expanded in the following form:

$$\Psi_n = V\alpha_n + W\beta_n + Y\zeta_n,\tag{6}$$

with Y defined analogous to V and W,

$$V^{\dagger}Y = W^{\dagger}Y = 0, \quad Y^{\dagger}Y = \mathbb{1}_r, \tag{7}$$

and coefficients α , β , and ζ are

$$\alpha_n = (\alpha_{n,1}, \alpha_{n,2}, \dots, \alpha_{n,r}),$$

$$\beta_n = (\beta_{n,1}, \beta_{n,2}, \dots, \beta_{n,r}),$$

$$\zeta_n = (\zeta_{n,1}, \zeta_{n,2}, \dots, \zeta_{n,r}).$$
(8)

By substituting hopping matrices $(J_{L,R})$ and superstate (Ψ_n) , respectively, from Eqs. (4) and (6), the right side of recursion relation (3) reduces to

$$E\Psi_n = \mathbf{K}[V\alpha_n + W\beta_n] + WX_R\alpha_{n-1} + VX_L\beta_{n+1}. \tag{9}$$

Here, we assume that the only relevant direction here is span $\{V\}$ and span $\{W\}$. The relation above can be reduced further by multiplying W^{\dagger} and V^{\dagger} from the left and making use of orthonormal relations (5). Then, we obtain

$$E\mathbb{1}_r\beta_n = K_{ww}\beta_n + X_R\alpha_{n-1} + K_{wv}\alpha_n, \tag{10}$$

$$E\mathbb{1}_r\alpha_n = K_{vv}\alpha_n + X_L\beta_{n+1} + K_{vw}\beta_n, \tag{11}$$

where $K_{ab} := A^{\dagger} \mathbf{K} B \in \operatorname{Mat}(r, \mathbb{C})$ with $A, B \in \{V, W\}$. In this formulation, the superlattice is restricted to the region $0 \le n \le 2L$, while the remaining sites represent the lead structure. Similar to the approach presented in [26], we model the lead's structure in the featureless wide-band limit, which is obtained by setting $K_{vw} = K_{wv} = X_R = X_L = w\mathbb{1}_r$ with w < 0 for $n \le 0$ (left lead), and $n \ge 2L$ (right lead). In addition, for each supersite in the lead, we tune the potential energy to the band center (i.e., $K_{ww} = K_{vv} = E\mathbb{1}_r$). Then, we can introduce the propagating modes, such as

$$\beta_n = \phi^{(+)} i^{n - n_+^{\beta}}, \quad \alpha_n = \phi^{(+)} i^{n - n_+^{\alpha}} \quad \text{(right)},$$

$$\beta_n = \phi^{(-)} (-i)^{n - n_-^{\beta}}, \quad \alpha_n = \phi^{(-)} (-i)^{n - n_-^{\alpha}} \quad \text{(left)}, \quad (12)$$

where the amplitude $\phi^{(\pm)} = (\phi_1^{(\pm)}, \dots, \phi_r^{(\pm)})$ are position-independent scattering modes throughout the lead's structure.

The possible noninteger offsets $n_{\pm}^{\alpha,\beta}$ can be chosen separately in each lead and account for the U(1) gauge freedom. We schematically demonstrate the lead's structure in Fig. 1.

B. Transport framework

As the main step to characterize the transport properties of the system, we construct the transfer matrix in the space of the real and propagating state. By introducing $\Phi_n = (\beta_n, \alpha_{n-1})^T$, we can define the transfer matrix M that connects the states in an adjacent supercell through the following relation:

$$\Phi_{n+1} = M_n \Phi_n. \tag{13}$$

In light of recursion relations (10) and (11), one can find the explicit form of the real-space transfer matrix as

$$M_{n} = \begin{pmatrix} X_{L}^{-1}[G_{vv}K_{wv}^{-1}G_{ww} - K_{vw}] & -X_{L}^{-1}G_{vv}K_{wv}^{-1}X_{R} \\ K_{wv}^{-1}G_{ww} & -K_{wv}^{-1}X_{R} \end{pmatrix},$$
(14)

where $G_{ab} = A^{\dagger}(E\mathbb{1}_r - \mathbf{K})B \in \operatorname{Mat}(r, \mathbb{C})$ with $A, B \in \{V, W\}$. The size of the transfer matrix depends on the rank of the hopping matrix \mathbf{J}_L . Then, the $2r \times 2r$ transfer matrix for the whole system can be given as

$$M = M_L \cdots M_3 M_2 M_1. \tag{15}$$

By considering the propagating mode (12) of the superlattice, the transfer matrix in the propagating-state basis is then defined by

$$\begin{pmatrix} \phi^{(+,R)} \\ \phi^{(-,R)} \end{pmatrix} = \mathcal{M} \begin{pmatrix} \phi^{(+,L)} \\ \phi^{(-,L)} \end{pmatrix}, \tag{16}$$

where L and R refer to the left and right lead. This transfer matrix captures the transport features in terms of linear relations between the propagating wave amplitudes in the leads. It is given by invoking the wave-matching condition of propagating waves. We then obtain

$$\mathcal{M} = \frac{1}{2} \begin{pmatrix} -i\mathbb{1}_r & \mathbb{1}_r \\ \mathbb{1}_r & -i\mathbb{1}_r \end{pmatrix} M \begin{pmatrix} i\mathbb{1}_r & \mathbb{1}_r \\ \mathbb{1}_r & i\mathbb{1}_r \end{pmatrix}. \tag{17}$$

In the next step, we can find the $r \times r$ right and left reflection and transmission matrices in terms of the entries of the transfer matrix \mathcal{M} in the propagating-state basis as

$$\begin{pmatrix} \mathbf{r} & \mathbf{t}' \\ \mathbf{t} & \mathbf{r}' \end{pmatrix}$$

$$= \begin{pmatrix} -\mathcal{M}_{22}^{-1} \mathcal{M}_{21} & \frac{\widetilde{\mathcal{M}}_{22} - \widetilde{\mathcal{M}}_{21} \widetilde{\mathcal{M}}_{11}^{-1} \widetilde{\mathcal{M}}_{12}}{|\mathcal{M}|} \\ \mathcal{M}_{11} - \mathcal{M}_{21} \mathcal{M}_{22}^{-1} \mathcal{M}_{21} & -\frac{\widetilde{\mathcal{M}}_{11}^{-1} \widetilde{\mathcal{M}}_{12}}{|\mathcal{M}|} \end{pmatrix}, \tag{18}$$

where $\widetilde{\mathcal{M}}_{ij}$ are the entries of the adjugate matrix of \mathcal{M} , and $|\mathcal{M}|$ is the determinant.

III. BOUNDARY CONDITIONS: GENERAL APPROACH

The transfer matrix approach in a real-space (M) and a scattering-state (\mathcal{M}) basis provides us with a comprehensive algorithm describing different boundary conditions for a variety of physical effects for the supermodel depicted in Fig. 1. This section defines various physical transport phenomena in the supermodel and demonstrates how we can characterize them using the transfer matrix method.

A. Periodic boundary conditions

The periodic boundary conditions for the system with L supercells require $\Psi_{n+N} = e^{ik_x}\Psi_n$. By considering decomposition of Ψ (6) and the definition of the transfer matrix (13), it leads to

$$M(E, k_{\perp})\Phi_n = e^{ik_x}\Phi_n. \tag{19}$$

Here, we consider a system in d spatial dimensions with open boundary conditions along the x-coordinate and periodic boundary conditions along the remaining d-1 directions, which are parametrized by the transverse quasimomentum $k_{\perp} \in \mathcal{T}^{d-1}$. This system can also be interpreted as a family of one-dimensional chains parametrized by k_{\perp} . Equation (19) reveals that the system with periodic boundary conditions has a state with complex energy E if and only if $e^{ik_x} \in \operatorname{Spec}[M(E, k_{\perp})]$. The complex spectrum of the system forms a closed curve in the complex plane, satisfying the following implicit dispersion equation:

$$\det (M(E, k_{\perp}) - e^{ik_x} \mathbb{1}_r) = 0.$$
 (20)

In the propagating-wave space, by considering the unitary transformation (17), the form of the implicit dispersion equation turns into

$$\det\left(\mathcal{M}(E, k_{\perp}) - e^{ik_x} \mathbb{1}_r\right) = 0. \tag{21}$$

B. Open boundary conditions

For the truncated system, the open boundary conditions can be fulfilled by setting $\Psi_0 = \Psi_{N+1} = 0$, which leads to $\alpha_0 = \beta_{L+1} = 0$ at the first sites of the leads. In terms of the real-space transfer matrix, the open boundary conditions imply

$$\begin{pmatrix} 0 \\ \alpha_N \end{pmatrix} = M(E, k_\perp) \begin{pmatrix} \beta_1 \\ 0 \end{pmatrix}, \tag{22}$$

which corresponds to

$$M_{11} = \mathbb{O}_r, \tag{23}$$

where \mathbb{O}_r is an $r \times r$ null matrix. The above relation can be read as r^2 separate implicit equations for the bound-state energies E_n , whose solutions are generally discrete but possibly complex.

C. Quasibound state and lasing

We define a quasibound state as a solution in which there only exists a purely outgoing wave (incoming waves are absent). This state can be achieved by setting $\phi^{(+,L)} = 0$ into the left lead and $\phi^{(-,R)} = 0$ into the right lead. In light of definition (16), to achieve a quasibound state, \mathcal{M}_{22} component

needs to fulfill

$$\mathcal{M}_{22}(E) = \mathbb{O}_r. \tag{24}$$

Generally, those solutions that satisfy the quasibound boundary conditions are discrete and complex. In a special case, these solutions present a stationary lasing state when their imaginary part is zero, i.e., $Im(E_n) = 0$.

D. Coherent perfect absorption

For the coherent perfect absorption (CPA), there is only a purely incoming wave (this corresponds to the time reversal of stationary lasing). Following the footsteps of the quasibound state boundary conditions, the CPA is achieved by setting $\phi^{(-,L)}=0$ into the left or $\phi^{(+,R)}=0$ into the right lead, which conduces to

$$\mathcal{M}_{11}(E) = \mathbb{O}_r. \tag{25}$$

E. Reflectionless, transparency, and invisibility

We define a reflectionless system from the left or right if the reflection matrix satisfies

$$\mathbf{r}(E) = \mathbb{O}_r \quad \text{or} \quad \mathbf{r}'(E) = \mathbb{O}_r.$$
 (26)

In terms of the transfer matrix, it can be expressed as

$$\mathcal{M}_{22}^{-1}\mathcal{M}_{21} = \mathbb{O}_r \quad \text{or} \quad \widetilde{\mathcal{M}}_{11}^{-1}\widetilde{\mathcal{M}}_{12} = \mathbb{O}_r.$$
 (27)

For the transparency condition, we consider just a phase shift for a probing wave passing through the system. In the language of the transmission matrix, depending on the side from which the system is probed, we have

$$\mathbf{t}(E) = \mathbb{O}_r \quad \text{or} \quad \mathbf{t}'(E) = \mathbb{O}_r,$$
 (28)

where in the context of the transfer matrix, it leads to

$$\mathcal{M}_{11} - \mathcal{M}_{21} \mathcal{M}_{22}^{-1} \mathcal{M}_{21} = (-i)^N \mathbb{1}_r$$
 or

$$\frac{\widetilde{\mathcal{M}}_{22} - \widetilde{\mathcal{M}}_{21} \widetilde{\mathcal{M}}_{11}^{-1} \widetilde{\mathcal{M}}_{12}}{|\mathcal{M}|} = (-i)^N \mathbb{1}_r.$$
 (29)

The system is invisible to the left (right) source if it is simultaneously reflectionless and transparent under illumination from that side. To be invisible to the detector, one needs to make the system reflectionless under illumination from that side and transparent under exposure from the other side.

IV. SPECIAL CASE: r = 1

A. Classification of transport effects

In this section, we focus on a specific case in which the rank of each of the hopping matrices $J_{L,R}$ is 1 (i.e., r=1), representing a family of tight-binding models, the most famous of which are two-band lattices, such as the Su-Schrieffer-Heeger (SSH) model. Other examples are the Chern insulator [34], 2D Dirac semimetal, and the Hofstadter model [35]. In such a special family, various qualitative topological properties of these systems can be extracted from the 2×2 transfer matrix [29,30]. Our approach can be extended to $r \neq 1$ models, but presenting an analytic framework will be challenging. In the

Appendix, we derive a 4×4 transfer matrix for one of these models.

For r = 1, the entries of the transfer matrix are given by complex-valued numbers, where the determinant is

$$d = \frac{K_{vw}X_R}{K_{wv}X_L}. (30)$$

From now on, K_{ab} , G_{ab} , and $X_{L,R}$ represent complex-valued numbers instead of matrices. For the Hermitian case [i.e., $\mathbf{K}^{\dagger}(E^*) = \mathbf{K}(E)$ and $X_R = X_L$], one can show that the determinant transforms to $d = K_{vw}(E)/K_{vw}^*(E^*)$. Therefore, in the Hermitian system, for the real energies, the determinant lies on the unit circle since $d = \exp[2i \arg K_{vw}(E)]$. One can reach the same result when the system is non-Hermitian, but couplings and on-site matrices are invariant under the parity (P) and time-reversal (T) operator. Then the determinant lies on the unit circle in the PT-unbroken phase. If we consider the system to be periodic, then by setting the unit-cell transfer matrix of the superlattice to M_c , the transfer matrix of the whole system with L supercell can be written as

$$M(E, k_{\perp}) = d^{L/2} [U_{L-1}(z)\overline{M}_c - U_{L-2} \mathbb{1}_{2 \times 2}],$$
 (31)

where $\overline{M}_c = M_c/\sqrt{d}$, $U_L(z)$ are the Chebyshev polynomials of the second kind, and

$$z = \text{tr}\overline{M}_c/2 = \frac{t}{2\sqrt{d}} = \frac{G_{vv}G_{ww} - K_{vw}K_{wv} - X_LX_R}{2\sqrt{K_{wv}K_{wv}X_LX_R}}.$$
 (32)

As a first consequence of the general formalism we introduced in this paper, one can formulate a set of boundary conditions for the particular case r = 1. In Table I, we characterize the transport properties of the system in terms of the entries of the transfer matrix and give the corresponding implicit equations.

In stationary transport phenomena such as reflectionless, transparency, and invisibility, real-valued energy is given. Hence the corresponding implicit equations in Table I can define the possible range of couplings or on-site potential for the given energy (or frequency) in which the system is in a stationary transport state. For other boundary conditions, the solutions of the corresponding implicit equations lead to a discrete complex spectrum describing quasistationary behavior.

There exists an alternative approach to obtain the spectrum related to open, quasiband, and scattering zero boundary conditions. Consider eigenstates and eigenenergies of the transfer matrix satisfying

$$M_c(E)\varphi_{1,2} = \rho_{1,2}\varphi_{1,2}.$$
 (33)

In the case of diagonalizable M_c , $\varphi_{1,2}$ form a basis of \mathbb{C}^2 in which one can expand Φ_N , and the coefficients can be defined by considering stationary boundary conditions [36]. For instance, the open boundary conditions (22) can be translated to

$$\begin{pmatrix} \beta_1 \\ 0 \end{pmatrix} = a_1 \varphi_1 + a_2 \varphi_2, \quad \begin{pmatrix} 0 \\ \alpha_N \end{pmatrix} = a_1 \rho_1^N \varphi_1 + a_2 \rho_2^N \varphi_2. \quad (34)$$

These equations reduce to a set of two complex homogeneous linear equations in terms of two variables a_1 and a_2 , satisfying

$$\sum_{l=1}^{2} a_{l} \mathcal{P}_{+} \varphi_{l} = \sum_{l=1}^{2} a_{l} \rho_{l}^{N} \mathcal{P}_{-} \varphi_{l} = 0,$$
 (35)

TABLE I. The second row of the table compares distinct boundary conditions (BCs) for a general model illustrated in Fig. 1 where the transfer matrix has to be taken as functions of energy E. For those models with r=1, the third row of the table characterizes implicit equations in terms of energy E for transport effects listed in the first row. The stationary situations correspond to given real energy, while those equations resulting in complex energies refer to quasistationary effects.

Boundary conditions	Characterization (arbitrary r)	Implicit equation $(r = 1)$
open	$M_{11}=\mathbb{O}_r$	$\sqrt{rac{d}{\kappa}}igg[rac{G_{vv}G_{ww}}{w^2}-\kappaigg]=rac{U_{L-2}(z)}{U_{L-1}(z)} \ t-de^{-ik_x}-e^{ik_x}=0$
periodic	$\det(M - e^{ik_x} \mathbb{1}_{2r \times 2r}) = 0$	$t - de^{-ik_x} - e^{ik_x} = 0$
quasibound	$\mathcal{M}_{22}=\mathbb{0}_r$	$U_{L-1}(z)\sqrt{\frac{d}{\kappa}}[(G_{vv}-iw)(G_{ww}-iw)-w^2\kappa]-2w^2U_{L-2}(z)=0$
CPA	$\mathcal{M}_{11}=\mathbb{0}_r$	$U_{L-1}(z)\sqrt{\frac{d}{\kappa}}[(G_{vv}+iw)(G_{ww}+iw)-w^2\kappa]-2w^2U_{L-2}(z)=0$
right-reflectionless	$\widetilde{\mathcal{M}}_{11}^{-1}\widetilde{\mathcal{M}}_{12}=\mathbb{0}_r$	$U_{L-1}(z)[(G_{ww}-iw)(G_{vv}+iw)-w^2\kappa]=0$
left-reflectionless	$\mathcal{M}_{22}^{-1}\mathcal{M}_{21}=\mathbb{0}_r$	$U_{L-1}(z)[(G_{ww} + iw)(G_{vv} - iw) - w^2\kappa] = 0$
right-invisible	$\begin{cases} \widetilde{\mathcal{M}}_{11}^{-1} \widetilde{\mathcal{M}}_{12} = \mathbb{O}_r, \\ \mathcal{M}_{11} - \mathcal{M}_{21} \mathcal{M}_{22}^{-1} \mathcal{M}_{21} = (-i)^N \mathbb{1}_r \end{cases}$	$\begin{cases} \sqrt{\frac{d}{\kappa}} [(G_{vv} - iw)(G_{ww} + iw) - w^2 \kappa] = \frac{(-i)^N d - 2w^2 U_{L-2}(z)}{U_{L-1}(z)}, \\ U_{L-2}(z) = -(-i)^N d \end{cases}$
left-invisible	$\begin{cases} \mathcal{M}_{22}^{-1}\mathcal{M}_{21} = \mathbb{O}_r, \\ \widetilde{\mathcal{M}}_{22} - \widetilde{\mathcal{M}}_{21}\widetilde{\mathcal{M}}_{11}^{-1}\widetilde{\mathcal{M}}_{12} \\ \mathcal{M} \end{cases} = (-i)^N \mathbb{1}_r$	$\begin{cases} \sqrt{\frac{d}{\kappa}} [(G_{vv} - iw)(G_{ww} - iw) - w^2 \kappa] = \frac{(-i)^N - 2w^2 U_{L-2}(z)}{U_{L-1}(z)}, \\ U_{L-2}(z) = -(-i)^N \end{cases}$

where $\mathcal{P}_{\pm}: \mathbb{C}^2 \to \mathbb{C}$ are projection operators that are defined as $\mathcal{P}_{+} = (0, 1)$ and $\mathcal{P}_{-} = (1, 0)$. They inject the state Φ into the subspaces β and α , respectively. Indeed, the open boundary condition (35) can be interpreted as the Dirichlet condition on the left edge, which is equivalent to the statement that Φ belongs to the range of \mathcal{P}_{+} , while the right edge is equivalent to the statement that the state Φ belong to the range of \mathcal{P}_{-} [29].

One can recast (35) in a matrix equation, which, according to Cramer's rule, has a nontrivial solution if

$$\det(\mathcal{R}_1^N \varphi_1 \,\mathcal{R}_2^N \varphi_2) = 0, \tag{36}$$

where

$$\mathcal{R}_l = \begin{pmatrix} \rho_l & 0\\ 0 & 1 \end{pmatrix}. \tag{37}$$

Equation (36) can be solved to get the set of energies for which the system with open boundary conditions has eigenstates.

Following the same approach for the quasibound and CPA boundary conditions, we obtain

$$\sum_{l=1}^{2} a_l \mathcal{P}_{\mp} \tilde{\varphi}_l = \sum_{l=1}^{2} a_l \rho_l^N \mathcal{P}_{\pm} \tilde{\varphi}_l = 0, \tag{38}$$

where the negative (positive) sign in each term refers to quasibound (CPA) boundary conditions, and $\tilde{\varphi}_l$ are the eigenstates of the transfer matrix in a propagating state, \mathcal{M} . They are given by

$$\tilde{\varphi}_l = \frac{1}{\sqrt{2}} \begin{pmatrix} i & 1\\ 1 & i \end{pmatrix} \varphi_l. \tag{39}$$

The corresponding energies can be obtained by finding the solutions of

$$\det(\mathcal{R}_1^N \tilde{\varphi}_1 \,\,\mathcal{R}_2^N \tilde{\varphi}_2) = 0 \tag{40}$$

for the CPA and

$$\det(\tilde{\mathcal{R}}_1^N \tilde{\varphi}_1 \ \tilde{\mathcal{R}}_2^N \tilde{\varphi}_2) = 0 \tag{41}$$

for the quasibound, where

$$\tilde{\mathcal{R}}_l = \begin{pmatrix} 1 & 0 \\ 0 & \rho_l \end{pmatrix}. \tag{42}$$

B. Compatibility of transport effects

In this section, we take a look at some of the aspects driven by the corresponding boundary conditions in the context of the transfer matrix. In addition to the determinant d, we introduce the following parameter:

$$\kappa = \frac{K_{vw}K_{wv}}{w^2}. (43)$$

As shown in Ref. [26], the two parameters d and κ play an important role in specifying the reciprocity and topology signature in the one-dimensional SSH model. Indeed, d quantifies the amount of nonreciprocity where the system becomes reciprocal and the non-Hermitian skin effect disappears for the parameter in which the transfer matrix is unimodular. The parameter κ represents the topological characteristic, with $\kappa = 1$ corresponding to the topological phase transition.

The transfer matrix (14) of the unit cell can be written in therms of the these parameters such as

$$M_c = \sqrt{\frac{d}{\kappa}} \begin{pmatrix} \frac{G_{vv}G_{ww}}{w^2} - \kappa & -\frac{G_{vv}}{w} \\ \frac{G_{ww}}{w} & -1 \end{pmatrix}. \tag{44}$$

Following the corresponding implicit equations from Table I for the right- and left-reflectionless transport yields

$$\mathcal{F}U_{L-1}(z) = 0, \tag{45}$$

with

$$\mathcal{F} = G_{vv}G_{ww} + w^2(1 - \kappa) \mp iw(G_{ww} - G_{vv}),$$
 (46)

where the minus (plus) sign applies to probing the system from the left (right). Condition (45) represents two different types of solutions where we interpret $[U_{L-1}(z) = 0]$ as a global and $(\mathcal{F} = 0)$ as a local mechanism. The solutions of the global mechanism given by the Chebyshev nodes depend on the length of the system L. If we set $E = K_{vv}$ or $E = K_{ww}$, which corresponds to $G_{vv} = 0$ or $G_{ww} = 0$, respectively [37], then from Eq. (32) one can find

$$z = -\frac{1}{2} \left(\sqrt{\kappa} + \frac{1}{\sqrt{\kappa}} \right). \tag{47}$$

It is easy to check that z remains intact under the transformation $\kappa \to 1/\kappa$ showing that the global mechanism for the reflectionless boundary conditions is also invariant under this transformation.

This is in contrast with the local mechanism. To reveal the difference between global and local mechanisms, consider probing the system from the left (right). Then the local condition leads to

$$w(1 - \kappa) = \pm i(K_{ww} - K_{vv}),$$
 (48)

where the plus (minus) sign gives left (right) -reflectionless. According to (48), in the local mechanism, κ shows up as an essential parameter for both left- and right-reflectionless boundary conditions.

To study other transport effects, we express the transfer matrix in the following form:

$$\tilde{\mathcal{M}} = \begin{pmatrix} \kappa_{+} + \frac{i\kappa_{-}\tilde{K}}{w(\kappa - 1)} & -i\kappa_{-} \left[1 - \frac{i\tilde{K}}{w(\kappa - 1)} \right] \\ i\kappa_{-} \left[1 + \frac{\tilde{K}}{w(\kappa - 1)} \right] & \kappa_{+} - \frac{i\kappa_{-}\tilde{K}}{w(\kappa - 1)} \end{pmatrix}, \tag{49}$$

where $\kappa_{\pm} := (\kappa^L \pm 1)$, $\tilde{K} := K_{ww} - K_{vv}$, and also we consider the normalized transfer matrix $\tilde{\mathcal{M}} := \frac{2\kappa^{L/2}}{(-1)^L d^{L/2}} \mathcal{M}$.

In particular, keeping the system reflectionless [i.e., requiring relation (48) to be satisfied], we can make it strictly transparent from the right (left) by setting $d = \kappa$ ($d = 1/\kappa$). The system is then invisible to a source (detector) placed to the system's reflectionless side.

For the CPA, employing the condition ($\mathcal{M}_{11}=0$) results in the following equation:

$$i(K_{ww} - K_{vv}) = -\frac{\omega \kappa_{+}(\kappa - 1)}{\kappa_{-}},\tag{50}$$

which is independent of the parameter d, and also invariant under the replacement $\kappa \to 1/\kappa$. One can simultaneously make the system transparent from the left by setting

$$d = (\kappa^{L/2} + \kappa^{-L/2})^{2/L}, \tag{51}$$

while it becomes transparent from the right if

$$d = (\kappa^{L/2} + \kappa^{-L/2})^{-2/L}.$$
 (52)

These results, we find in this section, have been spelled out in [26] for a one-dimensional nonreciprocal lattice, where the parameter d quantifies the amount of nonreciprocity and κ captures the topological characteristics in the SSH version. We present here a general version of the compatibility and

independence of transport effects for all those models categorized in the class of r=1. Hence, we can reexpress the transport behavior in more general terms such that (i) the direction of reflectionless transport depends on the parameter κ , (ii) invisibility coincides with the phase transition corresponding to $d=\kappa$ (d=1/k), where d measures the nonreciprocity of the system, and (iii) the coherent perfect absorption is compatible with the transparent effect.

C. Creutz ladder model

A general form of the nonreciprocal one-dimensional lattice is studied in [26] described by

$$E\psi_n = V_n \psi_n + u_n \psi_{n-1} + v_n \psi_{n+1}, \tag{53}$$

where V_n are on-site potentials, u_n are nearest-neighbor couplings from left to right, and v_n are nearest-neighbor couplings from right to left. In our formalism and notations, the hopping $\mathbf{J}_{L,R}$ and on-site \mathbf{K} matrices are given by

$$\mathbf{J}_{L} = \begin{pmatrix} 0 & 0 \\ v_{n} & 0 \end{pmatrix}, \ \mathbf{J}_{R} = \begin{pmatrix} u_{n-1} & 0 \\ 0 & 0 \end{pmatrix},$$
$$\mathbf{K} = \begin{pmatrix} V_{n-1} & u_{n} \\ v_{n-1} & V_{n} \end{pmatrix}, \tag{54}$$

which leads to the same transfer matrix expressed in relation (3) of Ref. [26]. We comprehensively explored the transport effect of this model in [26]. In this paper, we investigate the non-Hermitian one-dimensional Creutz ladder model depicted in Fig. 2. This model was introduced in [38] and has been studied in other subsequent papers [39–41]. Recently, a novel boundary-induced dynamical phenomenon, dubbed "edge burst," has been observed in the ladder lattice that possesses pure gain [11], which makes this model an interesting platform to be explored in both classical and quantum regimes.

A tight-binding lattice describes the Creutz ladder model with the following recursion relations:

$$E\psi_{n} = i\gamma\psi_{n} + u\psi_{n+1} + \frac{u'}{2}(\psi_{n-1} + \psi_{n+3}) + \frac{iu'}{2}(\psi_{n-2} - \psi_{n+2}),$$

$$E\psi_{n+1} = i\gamma'\psi_{n+1} + u\psi_{n} - \frac{iu'}{2}(\psi_{n-1} - \psi_{n+3})$$
(55)

$$E\psi_{n+1} = i\gamma'\psi_{n+1} + u\psi_n - \frac{1}{2}(\psi_{n-1} - \psi_{n+3}) + \frac{u'}{2}(\psi_{n-2} + \psi_{n+2}).$$
 (56)

The coupling and on-site matrices are then given by

$$\mathbf{J}_{L} = \begin{pmatrix} \frac{iu'}{2} & \frac{u'}{2} \\ \frac{u'}{2} & -\frac{iu'}{2} \end{pmatrix}, \ \mathbf{K} = \begin{pmatrix} i\gamma & u \\ u & i\gamma' \end{pmatrix}, \tag{57}$$

where one can see r = 1. Expanding in terms of orthonormal basis by using relation (6) gives

$$\Psi_n = \begin{pmatrix} \psi_{2n-1} \\ \psi_{2n} \end{pmatrix} = \frac{1}{\sqrt{2}} \begin{pmatrix} 1 \\ i \end{pmatrix} \alpha_n + \frac{1}{\sqrt{2}} \begin{pmatrix} i \\ 1 \end{pmatrix} \beta_n.$$
 (58)

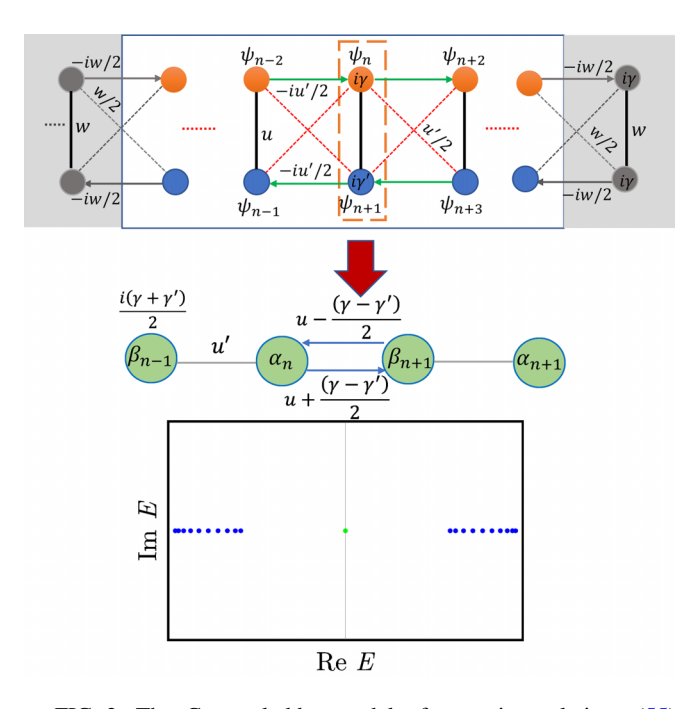


FIG. 2. The Creutz ladder model of recursion relations (55) and (56), which is connected to featureless leads from both sides. The lead's structure in the diagram can be achieved by following the relation (58) that transforms the Creutz ladder model to the non-Hermitian SSH model. This transformation reveals that the featureless leads ballistically attach to the Creutz model with the same structure by setting u = u' = w. In the case of balanced gain and loss (i.e., $\gamma = \gamma'$), the system is in the nontrivial topological phase if |u| < |w| and it supports a pair of degenerate zero edge modes shown by a green point in the complex energy spectrum of a finite ladder system with closed boundary conditions.

It transforms the recursions relations (59) and (60) to

$$E\beta_{n} = \frac{i(\gamma + \gamma')}{2}\beta_{n} + w\alpha_{n-1} + \left[u + \frac{(\gamma - \gamma')}{2}\right]\alpha_{n}, (59)$$

$$E\alpha_{n} = \frac{i(\gamma + \gamma')}{2}\alpha_{n} + w\beta_{n-1} + \left[u + \frac{(\gamma - \gamma')}{2}\right]\beta_{n}, (60)$$

which can also be achieved by making use of the general recursion formulas given in (10) and (11). Interestingly, the above equations describe a one-dimensional SSH model in Fig. 2. This unitary transformation has been discussed in other literature [6]. In fact, the reduction formalism leading to Eqs. (59) and (60) reveals that the transport properties of a non-Hermitian ladder model are given by those in a generic one-dimensional tight-binding lattice studied in [26] with the following on-site potentials:

$$V_{2n-1} = V_{2n} = \frac{i(\gamma + \gamma')}{2},\tag{61}$$

and couplings

$$u_{2n} = v_{2n-1} = u',$$

 $v_{2n} = u - \frac{(\gamma - \gamma')}{2}, \quad u_{2n} = u + \frac{(\gamma - \gamma')}{2}.$ (62)

In the following, we explore the transport effects and their compatibility in detail, but before that, we make a comment on the featureless leads attached to the ladder system.

At the beginning of this section, we remarked on the characteristics of the attached leads in a general formalism. This will give us a clue about the lead's structure. We consider a lead with a tight-binding structure similar to the ladder model whose parameter can be read from the projected one-dimensional SSH model. It then turns out that to make the featureless lead attached ballistically to the system, we need to set $E = i\gamma = i\gamma'$ and u = u' = w for the lead's sites. This is illustrated in Fig. 2.

For this system, the transfer matrix of the unit cell (44) is

$$M_c = \sqrt{\frac{d}{\kappa}} \begin{pmatrix} \frac{(E - i\bar{\gamma})^2}{w^2} - \kappa & \frac{-(E - i\bar{\gamma})}{w} \\ \frac{E - i\bar{\gamma}}{w} & -1 \end{pmatrix}, \tag{63}$$

where $\bar{\gamma} := (\gamma + \gamma')/2$, and d and κ are defined as

$$d = \frac{2u - (\gamma - \gamma')}{2u + (\gamma - \gamma')}, \qquad \kappa = \frac{4u^2 - (\gamma - \gamma')^2}{4W^2}.$$
 (64)

One can see that for $\gamma = \gamma'$, the system has a unimodular transfer matrix. In this case, the system becomes reciprocal, and the non-Hermitian skin effect vanishes.

To study the transport properties of this model, we start with reflectionless transport. The corresponding boundary conditions are expressed by Eq. (45). As we showed, the global mechanism is independent of transforming κ to $1/\kappa$, which connects the regions (κ < 1) and (κ > 1) in the ladder model. One then recalls that the system is topologically nontrivial with a pair of degenerate in-gap topological edge modes when [38]

$$\sqrt{\left|u^2 - \frac{(\gamma - \gamma')^2}{4}\right|} < |w|,\tag{65}$$

which become zero modes for $\gamma = -\gamma'$, or equivalently $\bar{\gamma} = 0$. This shows that the phase $(\kappa < 1)$ is a nontrivial topological phase where edge states do exist. Therefore, we realize that the global mechanism is essentially independent of the existence of edge states. This is analogous to what we found in [26] for the SSH model.

Now, let us turn to the local mechanism

$$0 = \mathcal{F} = (E - i\bar{\gamma})^2 + w^2(1 - \kappa). \tag{66}$$

Interestingly, the local mechanism yields the same relation for the left and right reflectionless conditions. If we set energy to the on-site potential, i.e., $E = \bar{E} = i\bar{\gamma}$, we then find that the system becomes reflectionless from both sides if $\kappa = 1$, corresponding to the topological phase transition

$$\sqrt{\left|u^2 - \frac{(\gamma - \gamma')^2}{4}\right|} = |w|. \tag{67}$$

Also, analogously to our findings in [26], the parameter d is absent in condition (67), which implies that the reflectionless transport is independent of nonreciprocity. In other words, the ladder model is reflectionless in both directions when

degenerate edge states relocalize via the skin effect to any edge of the system.

However, this termination might be different for other transport effects. To see this, we rewrite the total transfer matrix \mathcal{M} in the following form:

$$\mathcal{M} = \frac{(-1)^L d^{L/2}}{2\kappa^{L/2}} \begin{pmatrix} \kappa^L + 1 & -i(\kappa^L - 1) \\ i(\kappa^L - 1) & \kappa^L + 1 \end{pmatrix}.$$
(68)

Let us assume a system in the topological phase transition that is also reflectionless from both sides. Now, one can make it transparent from the right (left) by setting $d = \kappa$ $(d=1/\kappa)$. This condition also corresponds to $\gamma - \gamma' = \mathfrak{u}$ $(\gamma - \gamma' = -\mathfrak{u})$ with $\mathfrak{u} = |u - w|$ showing that the invisibility direction can be changed by interchanging $\gamma \leftrightarrow \gamma'$. This coincides precisely with the skin effect phase transition of a topological state. For CPA, applying the condition $\mathcal{M}_{11} = 0$ yields $\kappa = (-1)^{1/L}$. The transport effects can be tuned by manipulating the parameters of the model. We show this by considering an extended version of the Creutz ladder model, with coupling $u'e^{-i\theta}/2$ and $u'e^{i\theta}/2$ between adjacent sites in the different unit cell and $u \pm u_1$ between sites in a unit cell [41] (see Fig. 3). In this model, for the lattice with pure gain or loss (i.e., $\gamma = \gamma'$), the transfer matrix is unimodular (d = 1), while for the \mathcal{PT} -symmetric system (i.e., $\gamma = -\gamma'$), one can find

$$d = \frac{u - \gamma \sin \theta}{u + \gamma \sin \theta}.$$
 (69)

If |d|=1, there is no skin effect meaning that the "bulk states" decay into the bulk. These states are localized on the left boundary via the non-Hermitian skin effect for |d|<1, which results in $2\gamma\sin\theta<0$. For $\gamma>0$, this corresponds to $\theta\in[\pi,2\pi]$. For localizing on the right boundary, the determinant needs to satisfy |d|>1, leading to $2\gamma\sin\theta>0$, which includes $\theta\in[0,\pi]$. For the reflectionless transport, applying local mechanism $\mathcal{F}=0$ in Eq. (46) gives

$$w^2(1-\kappa) \pm 2wu_1\sin\theta$$

$$+\left(u\cos\theta - E - \frac{i(\gamma + \gamma')}{2}\right)^2 + u_1^2\sin^2\theta = 0.$$
(70)

For a better illustration, let us again set $E = \bar{E}$. Then we find that the system becomes reflectionless when

$$w^{2}(1-\kappa) = u^{2}(x^{2}-1) \mp 2wu_{1}x - u_{1}^{2}x^{2}, \tag{71}$$

where $x := \sin \theta$. For the reciprocal intercell coupling, i.e., $u_1 = 0$, the local mechanism gives

$$w^{2}(1-\kappa) = u^{2}(x^{2}-1). \tag{72}$$

The left-hand side is positive in the nontrivial topological phase (i.e., $\kappa < 1$). This requires $x^2 > 1$, implying that no solution exists for θ . Therefore, the system can only be made reflectionless in the trivial topological phase.

In the case of an extra degree of freedom $u_1 \neq 0$, the right-hand side of Eq. (71) is a quadratic equation whose behavior is determined by its discriminant

$$\Delta = 4u_1^2(w^2 - u^2) + 4u^4. \tag{73}$$

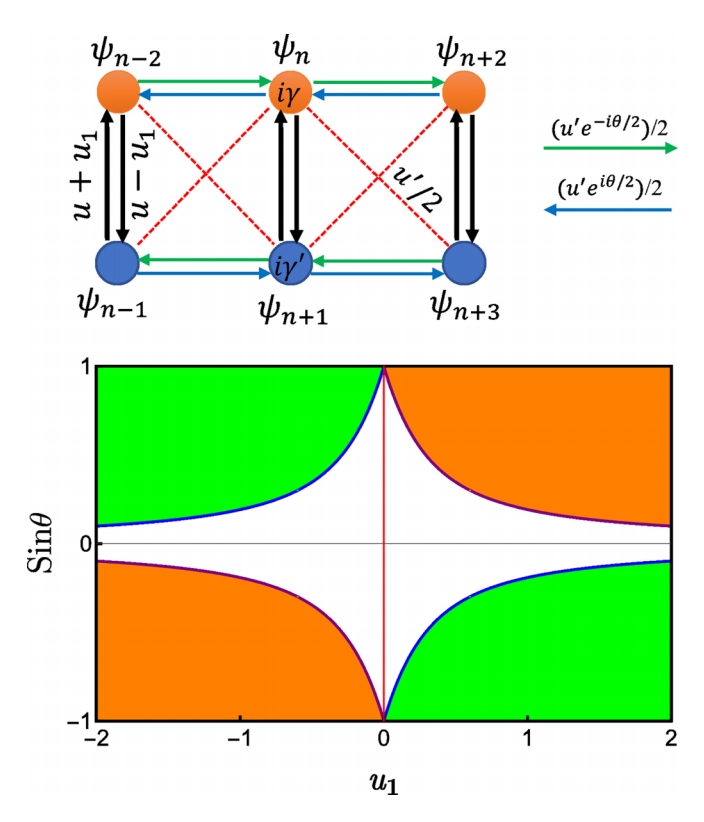


FIG. 3. The possible range for parameter $\theta = \arcsin x$, where the finite system displays left or right reflectionless boundary conditions in the nontrivial topological phase for the extended Creutz ladder illustrated schematically in the upper diagram. The blue curves locate the roots $x_{1,2}^r$ of Eq. (71) for the left reflectionless, while purple ones define the roots $x_{1,2}^r$ for the right reflectionless. The green and orange regions present a possible range for θ in terms of the nonreciprocity parameter u_1 where the system behaves reflectionless for the probe located on the right and left side, respectively. This plot shows that for a given $u_1 \in [-2, 2]/\{0\}$, one can find a possible range of θ that satisfies the local reflectionless condition. Those points along $u_1 = 0$ are excluded since the system cannot satisfy the reflectionless boundary conditions in the nontrivial topological phase.

If $\Delta > 0$, then there are two distinct real-valued roots x_1 and x_2 , and the right-hand side of Eq. (71) admits positive values for $x > x_2$ and $x < x_1$ where we supposed $x_1 < x_2$. For $-1 < x_1$ and $x_2 < 1$, one can find a possible range for θ such that the system satisfies the reflectionless boundary conditions. In Fig. 3, we plot a range of possible θ in which the system is reflectionless for the incoming wave from the left (right) in its nontrivial topological phase.

V. CONCLUSIONS

To summarize, we introduce a general formalism to establish transport effects and their interplays in a wide range of non-Hermitian, nonreciprocal, and potentially topological systems from a unifying scattering perspective. This work extends our previous work [26] to a general formalism applicable in concrete platforms with internal degrees of freedom or in higher dimensions.

For specific models, we reach a global characterization of transport boundary conditions presented in Table I, where we

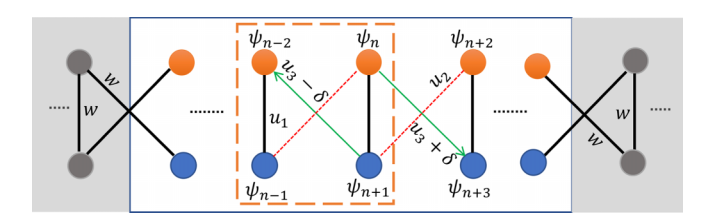


FIG. 4. A SSH model with alternating u_1 , u_2 couplings and a non-Hermitian $u_3 \pm \frac{\delta}{2}$ coupling fitting in r = 2 class.

can retrieve our findings for the compatibility of transport properties up to a system's parameters. The model's transport behavior can be predicted based on how those parameters are interpreted in different systems. The practical realization of these systems can be investigated in nonreciprocal photonics structures such as coupled resonant optical waveguides [16,42] where asymmetric coupling can be achieved by inserting an optical gain and loss medium into the link ring [43]. Furthermore, the method described in this paper can be used to tune the parameters of the topological system in order to obtain a specific transport effect. We demonstrated this by considering a generalized version of the ladder lattice in which one of the parameters can be set to a specific range to make it reflectionless in a nontrivial topological phase. A perspective of this approach can be studied in a two-dimensional lattice such as a non-Hermitian Chern insulator, a non-Hermitian 2D Dirac semimetal, or a non-Hermitian Hofstadter model. Also, a nonlinear extension version of the transfer matrix can be considered for studying the transport effect in the nonlinear SSH model [44].

ACKNOWLEDGMENTS

The work on this article was initiated and partially developed during my research position at Lancaster University, and I acknowledge support from EPSRC via Programme Grant No. EP/N031776/1 in that time. The author appreciates Henning Schomerus for coming up with the original idea in [26] and providing valuable comments and suggestions on this paper, and Delaram Mirfendereski for reading and editing the primary draft.

APPENDIX: TRANSFER MATRIX IN r = 2 CLASS

In this Appendix, we study the transfer matrix of a specific non-Hermitian Su-Schrieffer-Heeger (SSH) model whose rank of its hopping matrix is r = 2. The Bloch Hamiltonian of this model, which is depicted in Fig. 4,

reads [45]

$$H(k) = d_x(k)\sigma_x + d_y(k)\sigma_y, \tag{A1}$$

where $\sigma_{x,y}$ are Pauli matrices and

$$d_x(k) = u_1 + (u_2 + u_3)\cos k + i\frac{\delta}{2}\sin k,$$
 (A2)

$$d_{y}(k) = (u_2 - u_3)\sin k + i\frac{\delta}{2}\cos k.$$
 (A3)

One can read the hopping $(J_{L,R})$ and on-site (K) matrices as coefficients of e^{ik} and 1 in the Bloch Hamiltonian (A1), so that

$$\mathbf{J}_{L} = \begin{pmatrix} 0 & u_{3} + \delta \\ u_{2} & 0 \end{pmatrix}, \ \mathbf{J}_{R} = \begin{pmatrix} 0 & u_{2} \\ u_{3} - \delta & 0 \end{pmatrix},$$
$$\mathbf{K} = \begin{pmatrix} 0 & u_{1} \\ u_{1} & 0 \end{pmatrix}. \tag{A4}$$

The SVD results in (4) for $J_{L,R}$ with

$$V = \begin{pmatrix} 0 & 1 \\ 1 & 0 \end{pmatrix}, \quad W = \begin{pmatrix} 1 & 0 \\ 0 & 1 \end{pmatrix},$$

$$X_L = \begin{pmatrix} u_2 & 0 \\ 0 & u_3 + \delta \end{pmatrix}, \quad X_R = \begin{pmatrix} u_2 & 0 \\ 0 & u_3 - \delta \end{pmatrix}. \quad (A5)$$

It meets the requirement of our formalism in which the hopping matrices J_L and J_R differ only in their singular values [33]. The decomposition leads to the following entries of the unit-cell transfer matrix (14):

$$M_{11} = \begin{pmatrix} \frac{E^2}{u_1 u_2} & \frac{-2E}{u_2} \\ \frac{-2E}{u_3 + \delta} & \frac{E^2}{u_1 (u_3 + \delta)} \end{pmatrix}, M_{12} = \begin{pmatrix} \frac{-E}{u_1} & -\frac{u_3 - \delta}{u_2} \\ \frac{u_2}{u_3 + \delta} & \frac{-(u_3 - \delta)E}{u_1 (u_3 + \delta)} \end{pmatrix},$$

$$M_{21} = \begin{pmatrix} \frac{E}{u_1} & -1\\ -1 & \frac{E}{u_1} \end{pmatrix}, \quad M_{22} = \begin{pmatrix} -\frac{u_2}{u_1} & 0\\ 0 & \frac{-u_3 + \delta}{u_1(u_1)} \end{pmatrix}. \tag{A6}$$

The determinant of the transfer matrix is

$$d = \frac{u_3 - \delta}{u_3 - \delta},\tag{A7}$$

where the transfer matrix is unimodular for the vanishing nonreciprocal parameter δ , and the non-Hermitian skin effect vanishes [6]. To find the reflection and transmission matrices of the system in the propagating-state basis (16), one needs to attach the entire system to the leads from both sides. We demonstrated the structure of the leads in Fig. 4 using the formalism presented in this paper.

^[1] N. Moiseyev, *Non-Hermitian Quantum Mechanics* (Cambridge University Press, Cambridge, 2011).

^[2] T. Ozawa, H. M. Price, A. Amo, N. Goldman, M. Hafezi, L. Lu, M. C. Rechtsman, D. Schuster, J. Simon, O. Zilberberg, and I. Carusotto, Topological photonics, Rev. Mod. Phys. 91, 015006 (2019).

^[3] Y. Ashida, Z. Gong, and M. Ueda, Non-hermitian physics, Adv. Phys. 69, 249 (2020).

^[4] S. Yao and Z. Wang, Edge States and Topological Invariants of Non-Hermitian Systems, Phys. Rev. Lett. **121**, 086803 (2018).

^[5] S. Yao, F. Song, and Z. Wang, Non-Hermitian Chern Bands, Phys. Rev. Lett. 121, 136802 (2018).

^[6] S. Longhi, Probing non-hermitian skin effect and non-bloch phase transitions, Phys. Rev. Res. 1, 023013 (2019).

- [7] H. Schomerus, Nonreciprocal response theory of non-hermitian mechanical metamaterials: Response phase transition from the skin effect of zero modes, Phys. Rev. Res. 2, 013058 (2020).
- [8] K. Zhang, Z. Yang, and C. Fang, Correspondence between Winding Numbers and Skin Modes in Non-Hermitian Systems, Phys. Rev. Lett. 125, 126402 (2020).
- [9] N. Okuma, K. Kawabata, K. Shiozaki, and M. Sato, Topological Origin of Non-Hermitian Skin Effects, Phys. Rev. Lett. 124, 086801 (2020).
- [10] Y. Yi and Z. Yang, Non-Hermitian Skin Modes Induced by On-Site Dissipations and Chiral Tunneling Effect, Phys. Rev. Lett. 125, 186802 (2020).
- [11] W.-T. Xue, Y.-M. Hu, F. Song, and Z. Wang, Non-Hermitian Edge Burst, Phys. Rev. Lett. 128, 120401 (2022).
- [12] L. Lu, J. D. Joannopoulos, and M. Soljačić, Topological photonics, Nat. Photon. 8, 821 (2014).
- [13] M. Segev and M. A. Bandres, Topological photonics: Where do we go from here? Nanophotonics 10, 425 (2021).
- [14] H. Price, Y. Chong, A. Khanikaev, H. Schomerus, L. J. Maczewsky, M. Kremer, M. Heinrich, A. Szameit, O. Zilberberg, Y. Yang *et al.*, Roadmap on topological photonics, J. Phys. Photon. 4, 032501 (2022).
- [15] H. Schomerus, Quantum Noise and Self-Sustained Radiation of PT-Symmetric Systems, Phys. Rev. Lett. 104, 233601 (2010).
- [16] H. Zhao, P. Miao, M. H. Teimourpour, S. Malzard, R. El-Ganainy, H. Schomerus, and L. Feng, Topological hybrid silicon microlasers, Nat. Commun. 9, 1 (2018).
- [17] M. Parto, S. Wittek, H. Hodaei, G. Harari, M. A. Bandres, J. Ren, M. C. Rechtsman, M. Segev, D. N. Christodoulides, and M. Khajavikhan, Edge-Mode Lasing in 1D Topological Active Arrays, Phys. Rev. Lett. 120, 113901 (2018).
- [18] H. Ghaemi-Dizicheh, A. Mostafazadeh, and M. Sarısaman, Nonlinear spectral singularities and laser output intensity, J. Opt. 19, 105601 (2017).
- [19] H. Ghaemi-Dizicheh, A. Mostafazadeh, and M. Sarisaman, Spectral singularities and tunable slab lasers with 2d material coating, J. Opt. Soc. Am. B 37, 2128 (2020).
- [20] S. Longhi, \mathcal{PT} -symmetric laser absorber, Phys. Rev. A **82**, 031801(R) (2010).
- [21] Y. D. Chong, L. Ge, H. Cao, and A. D. Stone, Coherent Perfect Absorbers: Time-Reversed Lasers, Phys. Rev. Lett. 105, 053901 (2010).
- [22] C. Wang, W. R. Sweeney, A. D. Stone, and L. Yang, Coherent perfect absorption at an exceptional point, Science **373**, 1261 (2021),.
- [23] Z. Lin, H. Ramezani, T. Eichelkraut, T. Kottos, H. Cao, and D. N. Christodoulides, Unidirectional Invisibility Induced by PT-Symmetric Periodic Structures, Phys. Rev. Lett. 106, 213901 (2011).
- [24] R. El-Ganainy, K. G. Makris, M. Khajavikhan, Z. H. Musslimani, S. Rotter, and D. N. Christodoulides, Non-Hermitian physics and PT symmetry, Nat. Phys. 14, 11 (2018).
- [25] S. Longhi, D. Gatti, and G. Della Valle, Non-hermitian transparency and one-way transport in low-dimensional lattices by an imaginary gauge field, Phys. Rev. B **92**, 094204 (2015).
- [26] H. Ghaemi-Dizicheh and H. Schomerus, Compatibility of transport effects in non-Hermitian nonreciprocal systems, Phys. Rev. A **104**, 023515 (2021).
- [27] A. Mostafazadeh, Transfer matrix in scattering theory: A survey

- of basic properties and recent developments, Turk. J. Phys. 44, 472 (2020).
- [28] H. Schomerus, From scattering theory to complex wave dynamics in non-Hermitian PT-symmetric resonators, Philos. Trans. R. Soc. A **371**, 20120194 (2013).
- [29] V. Dwivedi and V. Chua, Of bulk and boundaries: Generalized transfer matrices for tight-binding models, Phys. Rev. B 93, 134304 (2016).
- [30] F. K. Kunst and V. Dwivedi, Non-hermitian systems and topology: A transfer-matrix perspective, Phys. Rev. B 99, 245116 (2019).
- [31] Z.-H. Wang, F. Xu, L. Li, D.-H. Xu, and B. Wang, Unconventional real-complex spectral transition and majorana zero modes in nonreciprocal quasicrystals, Phys. Rev. B 104, 174501 (2021).
- [32] G. Strang, *Introduction to Linear Algebra*, 4th ed. (Wellesley Cambridge Press, Wellesley, MA, 2009).
- [33] This formalism is based on the assumption that J_L and J_R are different just in their singular values as given in decomposition relation (4). In general, the decomposition approach fails for distinct right and left coupling matrices.
- [34] K. Kawabata, K. Shiozaki, and M. Ueda, Anomalous helical edge states in a non-hermitian chern insulator, Phys. Rev. B 98, 165148 (2018).
- [35] M. N. Chernodub and S. Ouvry, Fractal energy carpets in non-hermitian hofstadter quantum mechanics, Phys. Rev. E 92, 042102 (2015).
- [36] For a diagonalizable transfer matrix, the two modes $\varphi_{1,2}$ are linearly independent, and there is no coupling between them. However, in general, the transfer matrix is not normally referred to as a defective transfer matrix. Then a generalized form of expansion is required, with a coupling between two modes of the transfer matrix.
- [37] In the non-Hermitian nonreciprocal Su-Schrieffer-Heeger (SSH) lattice, K_{vv} and K_{ww} represent energies of localized zero edge modes.
- [38] T. E. Lee, Anomalous Edge State in a Non-Hermitian Lattice, Phys. Rev. Lett. 116, 133903 (2016).
- [39] F. K. Kunst, E. Edvardsson, J. C. Budich, and E. J. Bergholtz, Biorthogonal Bulk-Boundary Correspondence in Non-Hermitian Systems, Phys. Rev. Lett. 121, 026808 (2018).
- [40] V. M. Martinez Alvarez, J. E. Barrios Vargas, and L. E. F. Foa Torres, Non-hermitian robust edge states in one dimension: Anomalous localization and eigenspace condensation at exceptional points, Phys. Rev. B 97, 121401(R) (2018).
- [41] H.-Q. Liang and L. Li, Topological properties of non-hermitian creutz ladders, Chin. Phys. B **31**, 010310 (2022).
- [42] X.-Y. Zhu, S. K. Gupta, X.-C. Sun, C. He, G.-X. Li, J.-H. Jiang, X.-P. Liu, M.-H. Lu, and Y.-F. Chen, Z2 topological edge state in honeycomb lattice of coupled resonant optical waveguides with a flat band, Opt. Express 26, 24307 (2018).
- [43] X. Zhu, H. Wang, S. K. Gupta, H. Zhang, B. Xie, M. Lu, and Y. Chen, Photonic non-hermitian skin effect and non-bloch bulk-boundary correspondence, Phys. Rev. Res. **2**, 013280 (2020).
- [44] M. Reisner, D. H. Jeon, C. Schindler, H. Schomerus, F. Mortessagne, U. Kuhl, and T. Kottos, Self-Shielded Topological Receiver Protectors, Phys. Rev. Appl. 13, 034067 (2020).
- [45] F. Song, S. Yao, and Z. Wang, Non-Hermitian Topological Invariants in Real Space, Phys. Rev. Lett. 123, 246801 (2019).